Nonrenewable Resources, Vol. 5, No. 2, 1996

Fractal Pattern Integration for Mineral Potential Estimation

Qiuming Cheng,[1,3] F. P. Agterberg,[2] and G. F. Bonham-Carter[2]

Received January 18, 1996; accepted March 20, 1996

Concepts of fractal/multifractal dimensions and fractal measure were used to derive the prior and posterior probabilities that a small unit cell on a geological map contains one or more mineral deposits. This has led to a new version of the weights of evidence technique which is proposed for integrating spatial datasets that exhibit nonfractal and fractal patterns to predict mineral potential. The method is demonstrated with a case study of gold mineral potential estimation in the Iskut River area, northwestern British Columbia. Several geological, geophysical, and geochemical patterns (Paleozoic–Mesozoic sedimentary and volcanic clastic rocks; buffer zones around the contacts between sedimentary rocks and Mesozoic intrusive rocks; a linear magnetic anomaly; and geochemical anomalies for Au and associated elements in stream sediments) were integrated with the gold mineral occurrences which have fractal and multifractal properties with a box-counting dimension of 1.335 ± 0.077 and cluster dimension of 1.219 ± 0.037.

KEY WORDS: Fractal; multifractal; fractal measure; data integration; cluster dimension; GIS; mineral potential mapping.

INTRODUCTION

Geoscience maps of different types are to be integrated for target selection in mineral exploration. The geologist compares these maps and looks for combinations of indicators favorable for occurrence of mineral deposits of different types. The statistical integration of map data often involves the following stages: (1) superimposing grid cells of the same shape on a geological map; (2) coding relevant geological, geophysical, geochemical, and remote sensing features and mineral deposit information; and (3) modeling the association between the mineral deposits and the geoscience variables coded for each cell. Models constructed in this way are then used to predict undiscovered mineral deposits of the same type. The results obtained may depend strongly on the definitions of the variables used for the calculations and also on the arrangement, shapes, and sizes of the cells. In order to improve estimation, several types of approaches have been made; for example, various types of geoscience data can be extracted and associated according to a geological model locally characterizing the occurrence of mineral deposits (Harris, 1984; McCammon and others, 1983; Agterberg, 1989; Harris and Pan, 1991; Bonham-Carter and Chung, 1983; Bonham-Carter and Wright, 1989; Cheng, 1985; Cheng and Wang, 1990). Cell size and shape can be optimized; for example, irregularly shaped polygons, called "unique conditions" have been used by Agterberg and others (1990). These unique conditions represent real spatial objects characterized by unique geological conditions. Other efforts in this field include those by Cheng (1985), Cheng and Wang (1990), and Wang and others (1990) who also used geological objects instead of grid cells for sampling. In the latter studies, geological objects at different scales conceptually corresponding to ore

[1] Department of Earth and Atmospheric Science, York University, North York, Ontario M3J 1P3, Canada.
[2] Geological Survey of Canada, Ottawa K1A 0E8, Canada.
[3] Correspondence should be directed to Qiuming Cheng, Department of Earth and Atmospheric Science, York University, North York, Ontario M3J 1P3, Canada.

0961-1444/96/0600-0117$09.50/1

belts, ore fields, and ore deposits, were delineated on the geological map using synthesized (geological, geochemical, geophysical, and remote sensing) features and the favorability for mineralization and the amount of mineral resources were statistically estimated for each type of object.

The representation and calculation required for quantitative analysis of digitized patterns (points, lines, and areas) have been greatly aided by the development of geographical information systems (GIS) for the treatment of map data (Bonham-Carter, 1994; Bonham-Carter and others, 1988). In particular, the raster data model is available in most of GIS systems, which have the functionality to convert vector to raster formats suitable for data integration on the basis of unit cells or pixels. These and other GIS capabilities have led to the development of new methods for statistical and nonstatistical pattern integration, simulating the practice by exploration geologists of superimposing maps for delineating favorable areas. For instance, the weights of evidence method was proposed and has been intensively used for data integration (Agterberg, 1989, 1992; Agterberg and others, 1993b; Bonham-Carter 1994; Bonham-Carter and others, 1988; Cheng and others, 1994a). This method can be implemented by means of GIS on the basis of a polygon overlay map, called the unique conditions map, where each polygon represents a unique combination of the classes of input maps, although the calculations of the weights are performed by defining a fundamental unit area, or "unit cell." In addition, knowledge-based or subjective techniques have been used, including fuzzy set theory (An and others, 1991, 1992; Bonham-Carter, 1994; Cheng, 1986; Wright and Bonham-Carter, 1996) and the Dempster-Shafer model (Chung and Moon, 1991; Chung and Fabbri, 1993; An and others, 1994a, 1994b; Wright and Bonham-Carter, 1996). Fractal modeling was proposed for dealing with fractal and nonfractal patterns (Cheng, 1995; Cheng and others, 1994b). Implementation of these methods, especially for data-driven or objective models, usually employs measures on the map patterns, such as number of points, lengths of line segments, and areas of polygons. The required prior and conditional probabilities in weights of evidence modeling are estimated from the number of events (mineral deposits) and areas of indicator patterns. A commonly-used method is to superimpose a grid on the map which contains patterns of points, lines, and polygons for the features of interest, and then to count the number of cells containing these attributes. These numbers, from which the probabilities are estimated, depend on the cell size. In addition, it is usually assumed that the patterns are randomly located with respect to each small unit cell.

Fractal theory has shown that spatial patterns often exhibit non-integer dimension. For fractal patterns, the concepts of number, length, and area are not valid. In addition, as discussed by Cheng and Agterberg (1995), point patterns may have a spatial distribution with multifractal properties. "Ordinary" data integration methods can be modified to account for fractal properties. The purpose of this paper is to introduce a new procedure for fractal pattern integration. This method is demonstrated with a case study of Au mineral potential estimation in the Iskut River map sheet, northwestern British Columbia. The method can also be used for evaluating impact areas in environmental studies.

CHARACTERISTICS OF FRACTAL/ MULTIFRACTAL PATTERNS AND MEASUREMENTS

A fractal is a set with Hausdorff-Besicovitch dimension differing from its topological dimension (Mandelbrot, 1983; Cheng 1995). A classic example is the coastline. When a coastline is measured at progressively larger scales, its length generally increases infinitely. Applied to polygons, lines, and points, the ordinary measures of area, length, and number may be not valid if these objects are fractals. Figure 1A illustrates an artificial spatial object (black area) in a square region. The fractal dimension can be determined by box-counting as follows. A grid with variable cell size ϵ (1/2 to 1/32) is superimposed on the region. The number of cells containing the object, denoted as $N(\epsilon)$, is counted and represented in a log–log plot (figure 1B). A straight line fitted to these values has an estimated slope of -1.76. The corresponding estimate of the box-counting dimension is 1.76. In general, if the value $N_A(\epsilon)\epsilon^2$ approaches a finite value for small ϵ, it can be taken as the estimated area of nonfractal objects; $N_L(\epsilon)\epsilon$ and $N_E(\epsilon)$ are comparable measures of the length and number of nonfractal line and point objects, respectively. For fractal objects, however, $N(\epsilon)$ satisfies the following power–law relation (Mandelbrot, 1983):

$$N(\epsilon) = C\epsilon^{-D} \quad (1)$$

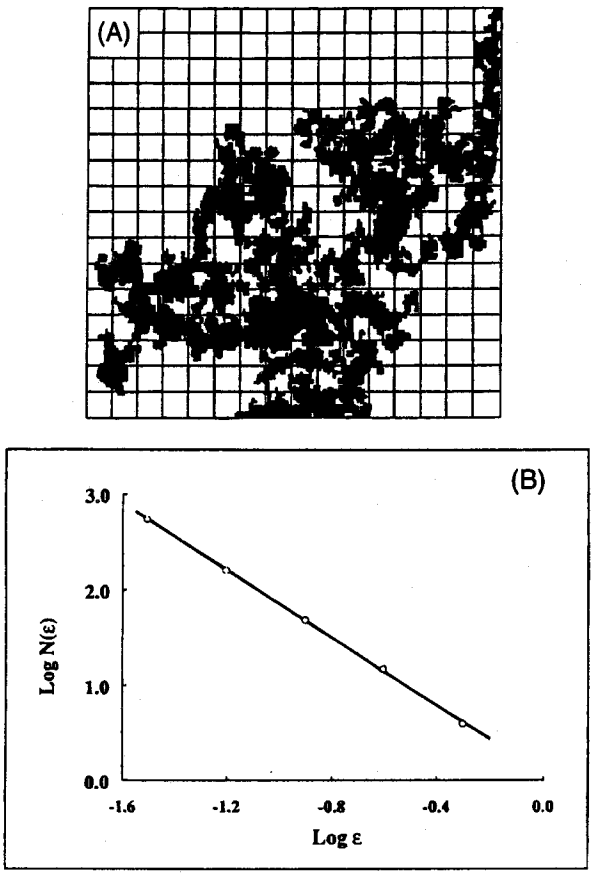

Figure 1. Artificial example showing fractal pattern and fractal measurements. (A) Fractal pattern is represented by black areas. Cell size is 1/16; (B) Log–log plot showing relationship between number of boxes containing the pattern for cell size ϵ (1/2, 1/4, 1/8, 1/16, 1/32). Straight line is least-squares fit, giving $D = 1.76$.

where $0 \leq D \leq 2$ is the box-counting dimension of the fractal pattern and c is a constant. This relation can be represented as a linear function on log–log paper:

$$\text{Log } N(\epsilon) = \text{Log } c - D \text{ Log } \epsilon \tag{2}$$

The dimension (D) is a useful measure for fractal patterns. Nonfractal geometries with integer dimensions can be considered as special fractal geometries. The constant c in equation 1 is also a measure of the geometry. For ordinary geometry c represents area with $D = 2$, length of line with $D = 1$, or number of points with $D = 0$. For fractals in D-dimensional space it is a measure of "size" that satisfies

$$c = \lim_{e-0} N(\epsilon)\epsilon^D \tag{3}$$

As a recent development of fractal theory, the concept of multifractal modeling has been applied in various fields of science for dealing with self-similar measures. For describing the characteristics of spatial patterns intersected with each cell, instead of using a binary measure for describing whether or not the cell contains an object, a more general measure can be defined, such as percentage of cell area occupied by the object. This measure to be denoted as $\mu(\epsilon)$, depends on cell size ϵ. If $\mu(\epsilon)$ is a multifractal measure, then its partition function

$$\chi_q(\epsilon) = \sum_{i=1}^{N(\epsilon)} \mu_i^q(\epsilon) \tag{4}$$

satisfies the following power–law relation for any $q(-\infty \leq q \leq \infty)$

$$\chi_q(\epsilon) \propto \epsilon^{\tau(q)} \tag{5}$$

where $N(\epsilon)$ represents the total number of cells containing the object. The parameter $\tau(q)$, called the "mass exponent," is a function of q. If $\tau(q)$ is a linear function of q, the multifractal reduces to a simple fractal; if it consists of finite straight line segments the multifractal can be called a discrete multifractal; and if $\tau(q)$ is a continuous function the multifractal is a continuous multifractal (cf. Cheng, 1995). Setting $q = 0$ in equation 5 gives

$$\chi_0(\epsilon) = N(\epsilon) \propto \epsilon^{\tau(0)} \tag{6}$$

for the partition function with box-counting dimension $D_E = -\tau(0)$. By setting $q = 1$, $q = 2$ in equation 5, the values of $\tau(1)$ and $\tau(2)$ can be estimated. These parameters can be used for characterizing the spatial distribution of the objects (for details see Cheng and Agterberg, 1995). In general, $\tau(1) = 0$ which expresses that the total "mass" $\chi_1(\epsilon)$ is independent of ϵ. Here this approach is used for a point set as follows.

Suppose a group of points E (mineral occurrences) in an area $S \subset \mathbf{R}^2$. The total number of points E may or may not be finite. Two cases can be considered: (1) the points in S have complete spatial randomness (CSR), or (2) the points E have a fractal/multifractal spatial distribution with a box-counting fractal dimension D_E and cluster fractal dimension $D_c = \tau(2)$. Various methods have been developed for testing the CSR assumption corresponding to a simple Poisson process (Ripley, 1981, 1988; Diggle, 1983; Cressie, 1991; Agterberg, 1994). In fractal methods (Mandelbrot, 1983; Feder, 1988; Carlson, 1991; Coleman and Pietronero, 1992; Cheng, 1995; Agterberg, 1994; Agterberg and others, 1993a), both the box-counting dimension D_E and cluster dimension D_C have

been used for describing the spatial properties of point processes. Multifractal modeling and associated spatial statistical methods can also be applied to point processes (Cheng, 1995; Cheng and Agterberg, 1995, submitted). Points satisfying a simple Poisson process with CSR have $D_E = -\tau(0) = 2$ and $D_C = \tau(2) = 2$; otherwise, $D_E = -\tau(0) < 2$ and $D_C = \tau(2) < 2$ indicating significant clustering. In order to construct a measure to characterize the distribution of points E which can be interpreted as a probability we need the following additional definitions.

Assume that a small cell u (without a lose of generality u can be taken as rectangular with size $\epsilon \times \epsilon$) is randomly taken from S. Three random variables can be defined: (1) the number of cells of size $\epsilon \times \epsilon$ covering the set S, to be denoted as N_s with expected value $EN_s = |S|/\epsilon^2$ where $|S|$ is the total area of set S; (2) the number of cells containing at least one point, denoted as N_g, which is a random variable with expected value $EN_\epsilon = N(\epsilon)$; and (3) the number of points in an area $A \subset S$, denoted as $N(A)$, which is a discrete random variable ($N(A) = 0, 1, \ldots, n$).

In the case of points with the CSR property, for any two sets $A \subset S$ and $B \subset S$ which do not intersect ($A \cap B = \phi$), $N(A)$ and $N(B)$ are independent random variables with binomial frequency distributions, e.g., for A:

$$P\{N(A) = k\} = \binom{n}{k}\left(\frac{|A|}{|S|}\right)k\left(1 - \frac{|A|}{|S|}\right)n - k \quad (7)$$

If $n >> 1$, equation 7 becomes a Poisson distribution

$$P\{N(A) = k\} \approx \frac{(\lambda|A|)^k}{k!} e^{-\lambda|A|} \quad (8)$$

where $\lambda = n/|S|$. Therefore, the probability of a small cell u containing one or more points is

$$\begin{aligned} P\{N(u) \geq 1\} &= 1 - P\{N(u) \\ &= 0\} \\ &= 1 - \left(1 - \frac{\epsilon^2}{|S|}\right)n \end{aligned} \quad (9)$$

or, from equation 8,

$$P\{N(u) \geq 1\} \approx 1 - e^{-\lambda\epsilon^2} \quad (10)$$

For small ϵ, equations 9 and 10 become approximately

$$P\{N(u) \geq 1\} \approx \frac{n}{|S|}\epsilon^2 \quad (11)$$

and

$$P\{N(u) \geq 1\} \approx \lambda\epsilon^2 \quad (12)$$

Either one of these two relations, which become identical for large n and small ϵ, is commonly used to estimate the probability $P\{N(u) \geq 1\}$. It will be shown that these relations have to be modified in the case of fractal points.

In order to generalize equations 11 and 12, the following relation between the variables N_s, N_ϵ, and $N(u)$ can be used

$$N_\epsilon = \sum_{i=1}^{N_s} I[N(u_i) - 1] \quad (13)$$

where $I[x]$ is the characteristic function with $I[x] = 1$, if $x \geq 1$; otherwise, $I[x] = 0$; u_i represents the i-th cell of size $\epsilon \times \epsilon$. The mean of N_ϵ can be estimated as follows (Cheng, 1989, 1995; Cheng and Wang, 1990). Writing the probability of N_s as $P\{N_s = k\}$, the conditional mean of N_ϵ given $N_s = k$ is

$$\begin{aligned} E[N_\epsilon|N_s = k] &= E\left[\sum_{i=1}^{k} I[N(u_i) - 1]\right] \\ &= kE\{I[N(u_i) - 1]\} = kP\{N(u) \geq 1\} \end{aligned} \quad (14)$$

Therefore,

$$\begin{aligned} N(\epsilon) &= E\{E[N_\epsilon|N_s = k]\} = \sum_k kP[N(u) \geq 1]P\{N_s = k\} \\ &= EN_sP\{N(u) \geq 1\} = N(S)P\{N(u) \geq 1\} \end{aligned} \quad (15)$$

and

$$P\{N(u) \geq 1\} \approx \frac{N(\epsilon)}{N(S)} \quad (16)$$

which is a generalization of equations 11 and 12. This is because for small ϵ, setting $N(\epsilon) \approx n$, it follows that $\lambda = n/|S|$ and equation 16 becomes identical to equations 11 and 12.

For fractal points with box-counting dimension D_E with $0 < D_E \leq 2$, theoretically,

$$N(\epsilon) \propto \epsilon^{-D_E} \quad (17)$$

where $N(\epsilon)$ increases infinitely as $\epsilon \to 0$. In this case, the total number of points (n) in S is infinite. Therefore, equations 11 and 12 can be replaced by equation 16. In practice, equation 16 holds true only for the limited range $\epsilon \in [\epsilon_{min}, \epsilon_{max}]$. It is affected by irregular edges for $\epsilon > \epsilon_{max}$ and by lack of map or computer resolution for $\epsilon < \epsilon_{min}$. For example, events may be located so close to one another that they cannot be represented

separately on a map with a given scale. In general, the magnitude of the total number of points does not necessarily represent a true property of the spatial distribution of the points. Therefore, equation 16 (with $\epsilon > \epsilon_{min}$ for a finite point set E) can be used for estimating the probability $P\{N(u) \geq 1\}$, and can be rewritten as

$$P\{N(u) \geq 1\} = \frac{C}{|S|} \epsilon^{2-D_E} \tag{18}$$

which no longer tends to a finite limit when $\epsilon \rightarrow 0$ if $D_E < 2$.

Figure 2 shows the locations of 183 Au mineral occurrences in the Iskut River map sheet, northwestern British Columbia. It was found that these points satisfy a multifractal model (Cheng, 1995; Cheng and Agterberg, 1995). The moment method of multifractal modeling can be used together with map analysis and spatial modeling by GIS. The estimated number of boxes containing one or more points is denoted as $N(\epsilon)$ and the density of points per cell with cell size ϵ (2–20 km) as $\mu(\epsilon)$. Figure 3 shows values of $\chi_q(\epsilon)$ calculated by equation 4 for $q = 0$ and 2. Straight lines were fitted to these values on log–log plots by means of least squares. It can be seen that when the cell size is too small (<4 km) the values of $\chi_0(\epsilon)$ depart from the straight line model. This is probably because events are then located so closely to one another that they could not be represented separately on the regional map with scale 1:250,000 that was used. For any map, if the unit cell is too small, $N(\epsilon)$ will asymptotically approach a constant value equal to the number of events (if this is a finite number). This implies that the power–law relation between $\chi_0(\epsilon)$ and ϵ is valid only to a minimum ϵ value. In figure 3 the slopes of the straight lines fitted to the values of $\chi_q(\epsilon)$ and ϵ (for $q = 0$ and 2) are $\hat{\tau}(0) = -1.335 \pm 0.077$ and $\hat{\tau}(2) = 1.219 \pm 0.037$, respectively, where the uncertainty is expressed using the standard deviation ($\pm s$). The difference between these values has an absolute value 2.554 ± 0.085 and is significantly greater than 0. It can be concluded that the points satisfy a multifractal instead of simple fractal model (cf. Cheng and Agterberg, 1995).

FRACTAL PATTERN INTEGRATION

Suppose that two patterns A and L are associated with the event E; for example, A may represent a rock

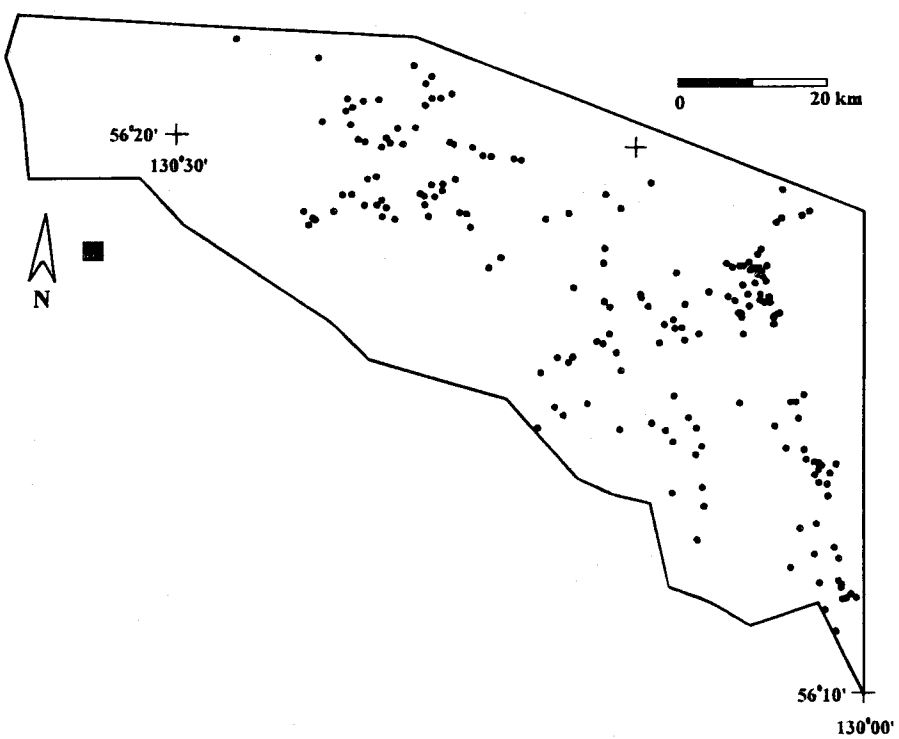

Figure 2. Mineral occurrences of gold in the Iskut River map sheet, northwestern British Columbia. Locations of 183 Au mineral occurrences represented by black dots.

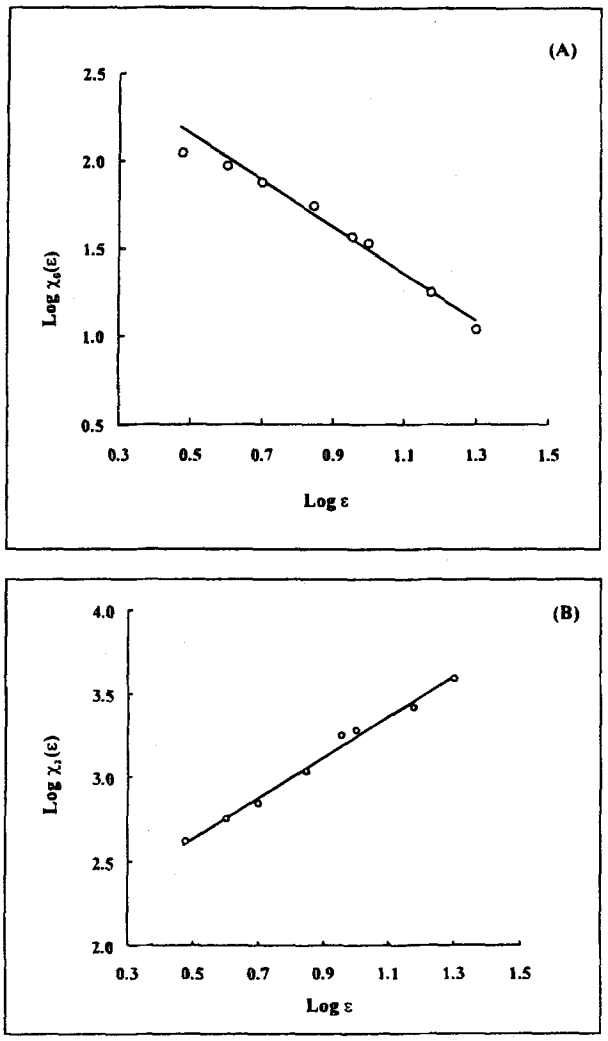

Figure 3. Log–log plots showing the relationships between $\chi_q(\epsilon)$ and ϵ according to eq. 4 with ϵ (20, 15, 10, 9, 7, 5, and 4 km). Straight lines are least-squares fits. (A) Relationship between $\chi_0(\epsilon)$ and ϵ, giving the box-counting dimension $\hat{\tau}(0) = -1.335 \pm 0.077$ and $c = 732 \pm 137.5$; (B) Relationship between $\chi_2(\epsilon)$ and ϵ, giving $\hat{\tau}(2) = 1.219 \pm 0.037$.

type and L a fault in a region while E represents mineral deposits of a given type. Let $P(E)$ represent the unconditional probability that a unit area contains one or more events (E), $P(E|A)$, $P(E|L)$ and $P(E|AL)$ be conditional probabilities for events occurring on the patterns A, L, and the overlap of A and L, respectively. They can be estimated using equation 16. Suppose further that A, L, E, and the various patterns of overlap of A, L, and E, have box-counting dimensions D_A, D_L, D_E, D_{AE}, D_{LE}, and D_{ALE} which have fractal or nonfractal dimensions depending on whether A, L, E, AE, LE, and ALE are fractals or nonfractal patterns. Then the numbers of cells containing these features can be expressed as:

$$\begin{aligned} N_A(\epsilon) &= C_A\epsilon^{-D_A} \\ N_L(\epsilon) &= C_L\epsilon^{-D_L} \\ N_E(\epsilon) &= C_E\epsilon^{-D_E} \end{aligned} \tag{19}$$

where c_A, c_L, and c_E are constants. Similarly, the expected numbers of cells containing A and E, L, and E, or A, L, and E are

$$\begin{aligned} N_{AE}(\epsilon) &= C_{AE}\epsilon^{-D_{AE}} \\ N_{LE}(\epsilon) &= C_{LE}\epsilon^{-D_{LE}} \\ N_{ALE}(\epsilon) &= C_{ALE}\epsilon^{-D_{ALE}} \end{aligned} \tag{20}$$

Therefore, using equation 16 the probabilities are estimated as:

$$\begin{aligned} P(E) &= \frac{C_E}{C_S}\epsilon^{2-D_E}; \quad P(\bar{E}) = 1 - \frac{C_E}{C_S}\epsilon^{2-D_E} \\ P(A) &= \frac{C_A}{C_S}\epsilon^{2-D_A}; \quad P(\bar{A}) = 1 - \frac{C_A}{C_S}\epsilon^{2-D_A} \\ P(L) &= \frac{C_L}{C_S}\epsilon^{2-D_L}; \quad P(\bar{L}) = 1 - \frac{C_L}{C_S}\epsilon^{2-D_L} \\ P(AE) &= \frac{C_{AE}}{C_S}\epsilon^{2-D_{AE}}; \quad P(LE) = \frac{C_{LE}}{C_S}\epsilon^{2-D_{LE}} \end{aligned} \tag{21}$$

where $c_s = |S|$, and the conditional probabilities are:

$$\begin{aligned} P(E|A) &= \frac{C_{AE}}{C_S}\epsilon^{D_A-D_{AE}}; \\ P(E|L) &= \frac{C_{LE}}{C_S}\epsilon^{D_L-D_{LE}} \\ P(E|\bar{A}) &= \frac{C_E\epsilon^{2-D_E} - C_{AE}\epsilon^{2-D_{AE}}}{C_S - C_A\epsilon^{2-D_A}}; \\ P(E|\bar{L}) &= \frac{C_E\epsilon^{2-D_E} - C_{LE}\epsilon^{2-D_{LE}}}{C_S - C_L\epsilon^{2-D_L}} \end{aligned} \tag{22}$$

These relationships between A, L, and E can be summarized by a ($2 \times 2 \times 2$) table of probabilities (table 1). Conditional independence of A and L given E implies:

$$\begin{aligned} P(AL|E) &= P(A|E)P(L|E); \\ P(\bar{A}L|E) &= P(\bar{A}|E)P(L|E) \\ P(A\bar{L}|E) &= P(A|E)P(\bar{L}|E); \\ P(\bar{A}\bar{L}|E) &= P(\bar{A}|E)P(\bar{L}|E) \end{aligned} \tag{23}$$

Table 1. Relationships Between A, L, and E

	E		$\bar{E}$	
	L	$\bar{L}$	L	$\bar{L}$
A	$P(ALE)$	$P(A\bar{L}E)$	$P(AL\bar{E})$	$P(A\bar{L}\bar{E})$
$\bar{A}$	$P(\bar{A}LE)$	$P(\bar{A}\bar{L}E)$	$P(\bar{A}L\bar{E})$	$P(\bar{A}\bar{L}\bar{E})$

The relations of equation 23 are equivalent to:

$$C_{ALE} = \frac{C_{AE}C_{LE}}{C_E}; \quad D_{ALE} = D_{AE} + D_{LE} - D_E$$

$$C_{A\bar{L}E} = \frac{C_{AE}C_{\bar{L}E}}{C_E}; \quad D_{A\bar{L}E} = D_{AE} + D_{\bar{L}E} - D_E$$

$$C_{\bar{A}LE} = \frac{C_{\bar{A}E}C_{LE}}{C_E}; \quad D_{\bar{A}s} = D_{\bar{A}E} + D_{LE} - D_E \quad (24)$$

$$C_{\bar{A}\bar{L}E} = \frac{C_{\bar{A}E}C_{\bar{L}E}}{C_E}; \quad D_{\bar{A}\bar{L}E} = D_{\bar{A}E} + D_{\bar{L}E} - D_E$$

If the assumption of conditional independence of A and L holds true, the eight probabilities in the preceding table are mutually interrelated by:

$$\begin{aligned} P(ALE) &= P(A|E)P(L|E)P(E) \\ P(AL\bar{E}) &= P(A|\bar{E})P(L|\bar{E})P(\bar{E}) \end{aligned} \quad (25)$$

If odds (O) are used instead of probabilities (P) with $O = P/(1 - P)$, then:

$$\begin{aligned} \log_e O(E|AL) &= W_A^+ + W_L^+ + \log_e O(E) \\ \log_e O(E|\bar{A}) &= W_A^- + W_L^+ + \log_e O(E) \\ \log_e O(E|A\bar{L}) &= W_A^+ + W_L^- + \log_e O(E) \\ \log_e O(E|\bar{A}\bar{L}) &= W_A^- + W_L^- + \log_e O(E) \end{aligned} \quad (26)$$

These are extensions of Bayes' rule which holds only if A and L are conditionally independent. The weights

$$W_A^+ = \log\left\{\frac{P(A|E)}{P(A|\bar{E})}\right\}; \quad W_A^- = \log\left\{\frac{P(\bar{A}|E)}{P(\bar{A}|\bar{E})}\right\}$$

$$W_L^+ = \log\left\{\frac{P(L|E)}{P(L|\bar{E})}\right\}; \quad W_L^- = \log\left\{\frac{P(\bar{L}|E)}{P(\bar{L}|\bar{E})}\right\} \quad (27)$$

satisfy the following expressions:

$$W_A^+ \propto \log\left[\frac{\frac{C_{AE}}{C_E}\epsilon^{D_E - D_{AE}}}{\frac{C_A - C_{AE}\epsilon^{2-D_{AE}}}{C_S - C_E\epsilon^{2-D_E}}}\right]$$

$$\sim \log\left[\frac{C_{AE}C_S}{C_AC_E}\epsilon^{D_E - D_{AE}}\right]$$

$$W_A^- \propto \log\left[\frac{1 - \frac{C_{AE}}{C_E}\epsilon^{D_E - D_{AE}}}{1 - \frac{C_A - C_{AE}\epsilon^{2-D_{AE}}}{C_S - C_E\epsilon^{2-D_E}}}\right] \quad (28)$$

$$\sim \log\left[\frac{C_S - \frac{C_{AE}}{C_E}\epsilon^{D_E - D_{AE}}}{C_S - C_A}\right]$$

It shows that $C_A = W_A^+ - W_A^-$ (more details about the definition of the contrast C can be found in Agterberg and others, 1990) decreases as ϵ decreases ($C_A \propto \log \epsilon$), because, in general, $D_{AE} < D_E$. W_A^+ and W_A^- are independent of ϵ only if $D_{AE} \approx D_E$ or if $D_E = 0$ for a nonfractal point pattern. In this special case, W_A^+ and W_A^- can be calculated using c_{AE}, c_E, c_A, and c_S. For small ϵ and $D_A = 2$, we have the following approximation:

$$\log O(E|A) - W_A^+ + \log\left\{\frac{C_E}{C_S}\epsilon^{2-D_E}\right\} \quad (29)$$

or

$$O(E|A) \sim \frac{C_{AE}}{C_A}\epsilon^{2-D_{AE}} \quad (30)$$

Then $O(E|A)$ has a power-law relation with cell size ϵ with exponent $2 - D_{AE}$.

Standard deviations of the weights W_A^+ and W_A^- can be obtained as follows (cf. Bishop and others, 1975; Agterberg, 1992):

$$\begin{aligned} s^2(W_A^+) &= \frac{1}{N_{AE}(\epsilon)} + \frac{1}{N_{A\bar{E}}(\epsilon)} \\ s^2(W_A^-) &= \frac{1}{N_{A\bar{E}(\epsilon)}} + \frac{1}{N_{\bar{A}E}(\epsilon)} \end{aligned} \quad (31)$$

which can be rewritten using equations 19 and 20 as:

$$s^2(W_A^+) = \frac{C_A}{(C_A - C_{AE}\epsilon^{D_A - D_{AE}})C_{AE}\epsilon^{-D_{AE}}}$$

$$s^2(W_A^-) = \frac{C_S - C_A\epsilon^{2-D_A}}{(C_E\epsilon^{-D_E} - C_{AE}\epsilon^{-D_{AE}})(C_S - C_E\epsilon^{2-D_E} - C_A\epsilon^{2-D_A} + C_{AE}\epsilon^{2-D_{AE}})} \quad (32)$$

Both $s(W_A^+)$ and $s(W_A^-)$ decrease as ϵ decreases. However, the standardized value of $C(t(C) = C/s(C))$ is approximately $t(C) \propto \epsilon^{-1/2DE}$ which increases as ϵ decreases. Therefore, the optimum cell size ϵ should be the smallest possible value for which (a) the power-law relations of the fractal patterns hold true, and (b) $t(C)$ is as large as possible.

GOLD POTENTIAL ESTIMATION FOR THE ISKUT RIVER MAP SHEET, NORTHWESTERN BRITISH COLUMBIA

Indicator Patterns and Fractal Characteristics

The area chosen for this study is the Iskut River map sheet (NTS104B), northwestern British Columbia. Geological variables were selected by metallogenic considerations and probabilistic approaches based on fundamental geological principles of hydrothermal deposit formation, combined with regional geochemical, geophysical, and mineral inventory data (data from Geological Survey of Canada, 1978, 1988). The datasets used for this study consist of (a) geological map (1:250,000); (b) regional geochemical reconnaissance data (1:250,000); (c) regional aeromagnetic data (1:250,000); and (d) mineral occurrence records (B.C. Minfile, 1989). For the present study, the following indicator patterns will be considered: (1)Paleozoic–Mesozoic sedimentary and volcanic clastic rocks (figure 4A); (2) buffer zones (<10 km) around the contacts between Paleozoic–Mesozoic sedimentary and volcanic clastic rocks and Mesozoic intrusive rocks (quartz diorite, monzonite, monzodiorite, and alkali-feldspar porphyry intrusions) (see figure 4B); (3) magnetic anomaly lows (<36.9 Nt) (see figure 4C); and (4) geochemical anomalies for Au (>30 ppb) in stream sediments (figure 4D).

The binary pattern in figure 4A was compiled using Voronoi tessellation based on the geological units coded for 698 stream sediment stations. Buffer zones in figure 4B and binary aero-magnetic patterns in figure 4C were delineated and optimized in terms of the contrast $C = W^+ - W^-$ (cf. Agterberg, 1989, 1992), respectively. Gold anomalies in figure 4D were delineated by statistical and fractal methods (Cheng, 1995; Cheng and others, 1994d, 1995). To use the method introduced in this paper for integrating these binary patterns (figure 4A–D) with Au mineral occurrences (figure 2), the box-counting method for different cell sizes (2–20 km) was used for estimating the fractal dimensions and related measures. The estimated results for the Au mineral occurrences on the overlaps of the binary patterns are shown in figure 5 and the estimated fractal measurements are summarized in table 2. The binary patterns of figure 4A–D were considered to be ordinary nonfractal polygon patterns by setting $D = 2$ and assigning constant measure c to the polygon areas.

Table 2. Fractal Measurements for the Binary Patterns, X_1 to X_4

Geological features	Label	D	c
Au mineral occurrences	E	1.335 ± 0.077	732 ± 137.5
P-M sedimentary rock	X_1	2	2387
Buffers around contacts	X_2	2	3144
Magnetic anomalies	X_3	2	1128
Au geochem. anomalies	X_4	2	2241
	$E\&X_1$	1.246 ± 0.047	401 ± 44.0
Overlap conditions	$E\&X_2$	1.289 ± 0.069	514 ± 84.8
	$E\&X_3$	0.902 ± 0.059	124 ± 17.5
	$E\&X_4$	1.223 ± 0.075	428 ± 78.0
Basemap	S	2	4754

Pattern Integration

The mineral occurrences on each binary pattern can be treated as fractal sets (figure 5A–D). The fractal measures for these sets as estimated by means of the box-counting method become dimensions (D from 0.9023 to 1.2885) and measures (c from 123.83 to 513.94) which are less than the dimension ($D = 1.335 \pm 0.077$), and measure ($c = 732.46 \pm 137.5$) for all occurrences. From the estimated values of D and c, the weights (W^+ and W^-) and their standard deviations ($s(W^+)$ and $s(W^-)$) can be calculated for each pattern by equations 28 and 32. The results obtained for each binary pattern using cell sizes 1, 2, 4, 6, and 8 (km) are shown in tables 3 and 4. Generally, the weights (W^+ and W^-) and their standard deviations ($s(W^+)$ and $s(W^-)$) decrease but the t-values increase as cell size decreases.

For comparison, the ordinary weights of evidence method was used to compute the weights for the binary patterns. The results for binary rock patterns (figure

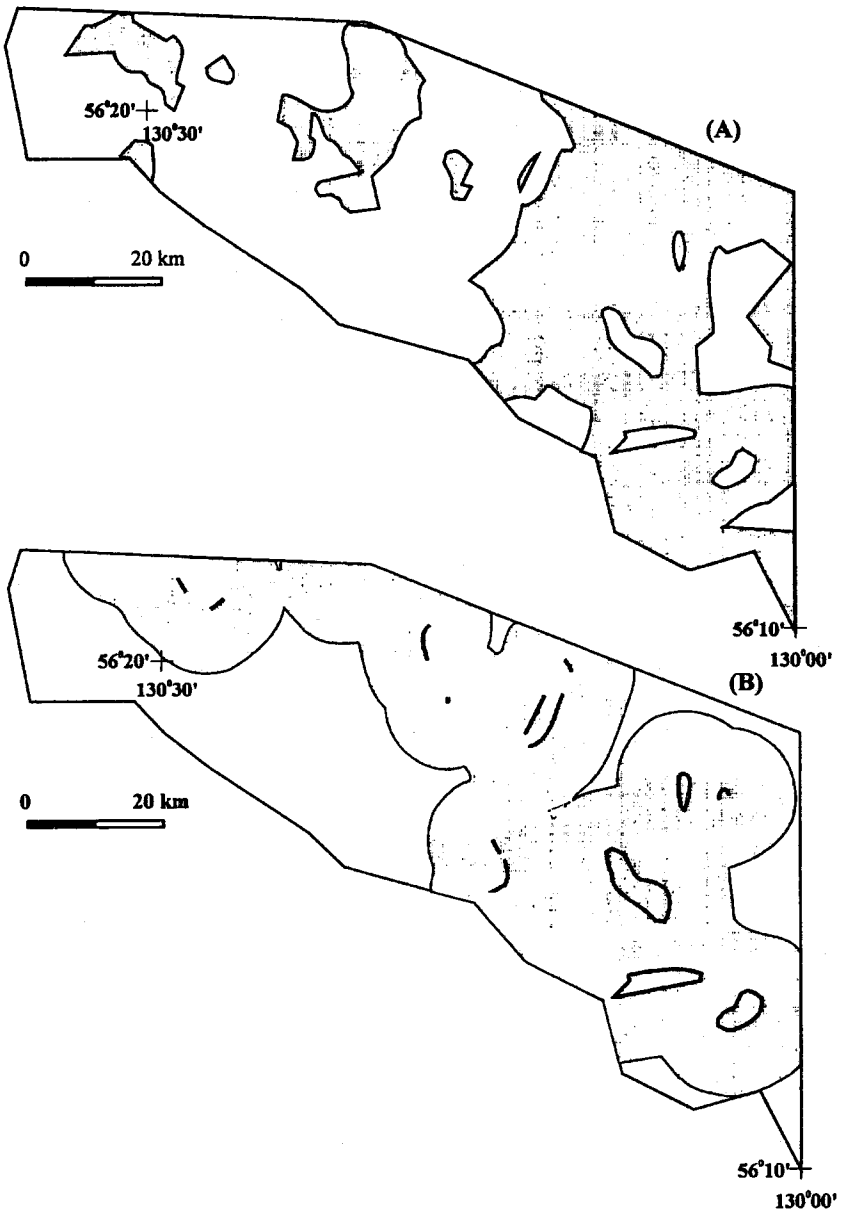

Figure 4. Indicator patterns (shaded areas) for Au mineral potential mapping. (A) Paleozoic to Mesozoic sedimentary and volcaniclastic rocks; (B) Buffer zones around the contacts between Paleozoic to Mesozoic rocks in (A) and Mesozoic intrusive rocks (quartz diorite, monzonite, monzodiorite, alkali-feldspar porphyry intrusions)(10 km on both sides). Solid curves represent contacts; (C) Aeromagnetic anomalies (<39.6 Nt) delineated by optimizing contrast C (cf. Agterberg and others 1990); (D) Geochemical anomalies for Au (>30 ppb) in stream sediments delineated by fractal and spatial statistical methods (Cheng and others, 1994d, 1994e).

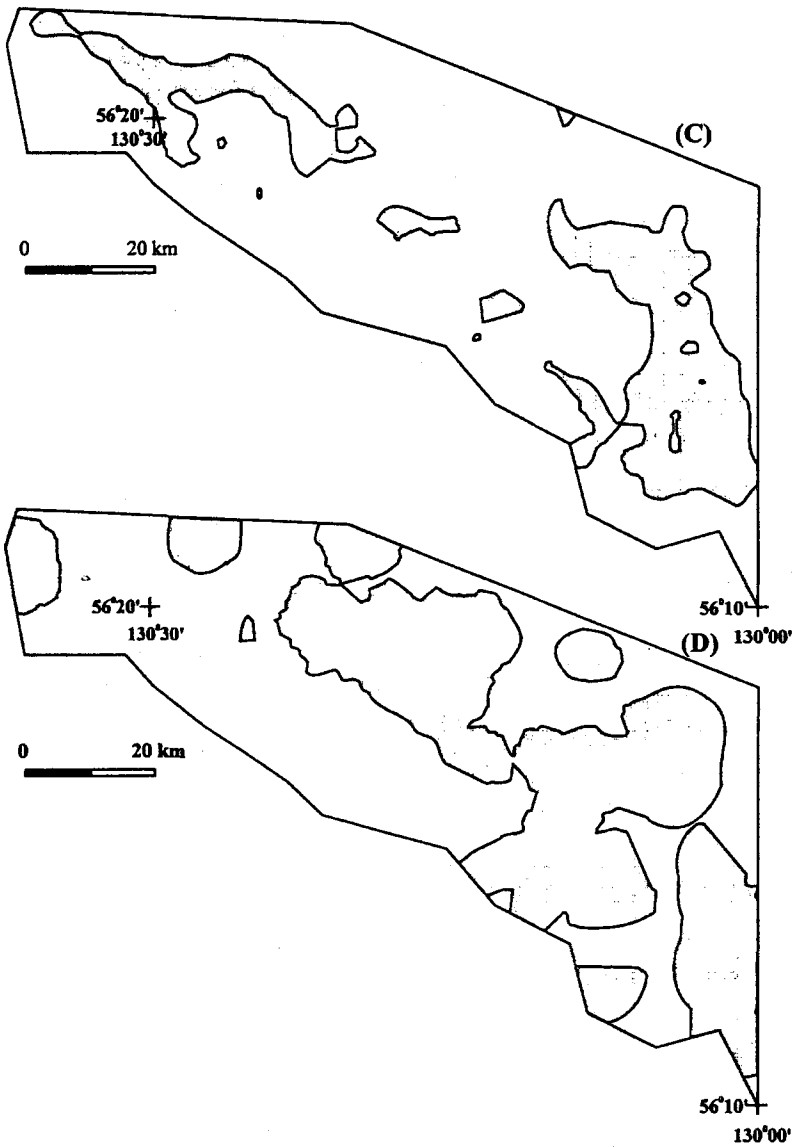

Figure 4. Continued

Table 3. Comparison of Weights for Binary Rock Patterns Shown in figure 4a ($s_1 = s(W^+)$ and $s_2 = S(W^-)$)

	Ordinary weights					Fractal weights				
ϵ^2	W^+	s_1	W^-	s_2	$t(C)$	W^+	s_1	W^-	s_2	$t(C)$
8	.58	.12	−.78	.16	6.65	.53	.41	−.48	.36	1.84
6	.47	.11	−.69	.15	6.24	.34	.26	−.37	.28	1.85
4	.42	.10	−.65	.15	5.94	.21	.16	−.25	.19	1.84
2	.37	.09	−.60	.14	5.83	.11	.09	−.13	.11	1.69
1	.36	.09	−.59	.14	5.71	.04	.05	−.05	.06	1.14

4A) with different unit cells are shown in table 3. It can be seen that the weights obtained by means of the ordinary and fractal weights of evidence methods with various unit cells decrease as cell size ϵ decreases. The difference between the results obtained by the two methods is that the t-values obtained by the fractal method increase when $\epsilon > \epsilon_{min}$, whereas the t-value obtained by the ordinary weights of evidence slightly decreases or tends to become constant as the cell unit ϵ decreases. The reason for this is that the ordinary method assumes $D_E = 0$ whereas the fractal method uses $D_E = 1.335$. As pointed out before, the optimum

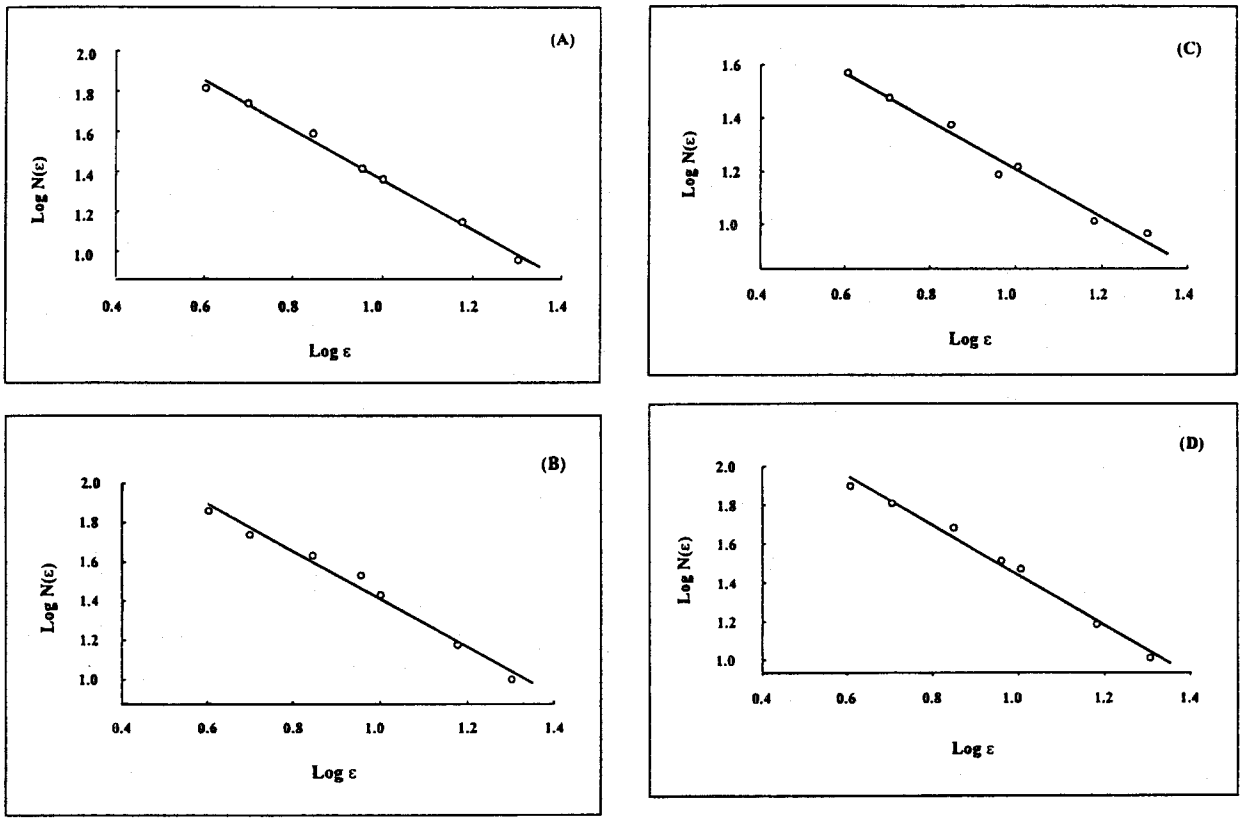

Figure 5. Log–log plots showing fractal analysis for mineral occurrences on the binary patterns in figure 4, respectively. Straight lines are least-squares fits. Cell sizes used are 20, 15, 10, 9, 7, 5, and 4 km. The estimates of fractal measures (D and c) are shown in table 2.

Table 4. Weights for Binary Patterns Obtained Using Fractal Method

X	ϵ(km)	W^+	$s(W^+)$	W^-	$s(w^-)$	C	$s(C)$	$t(C)$
X_1	8	0.5342	0.4128	−0.4792	0.3643	1.0134	0.5505	1.8408
	6	0.3370	0.2571	−0.3654	0.2787	0.7024	0.3792	1.8520
	4	0.2136	0.1639	−0.2517	0.1931	0.4653	0.2533	1.8375
	2	0.1090	0.0909	−0.1270	0.1056	0.2360	0.1393	1.6940
	1	0.0440	0.0548	−0.0479	0.0592	0.0920	0.0806	1.1404
X_2	8	0.3252	0.3169	−0.6550	0.4895	0.9802	0.5832	1.6809
	6	0.2215	0.2171	−0.5805	0.3669	0.7220	0.4261	1.6942
	4	0.1457	0.1438	−0.3448	0.2486	0.4905	0.2872	1.7078
	2	0.0757	0.0806	−0.1730	0.1325	0.2487	0.1550	1.6041
	1	0.0304	0.0482	−0.0641	0.0728	0.0946	0.0873	1.0833
X_3	8							
	6	0.6343	0.4346	−0.1834	0.2080	0.8178	0.4818	1.6972
	4	0.2584	0.2382	−0.0778	0.1433	0.3362	0.2780	1.2455
	2	0.0001	0.1405	−0.0000	0.0784	0.0000	0.1608	0.0012
	1	−0.1694	0.0952	0.0443	0.0444	−.2137	0.1051	−2.0330
X_4	8	1.3118	0.8729	−0.7515	0.4195	2.0630	0.9685	2.1305
	6	0.5940	0.3005	−0.5816	0.3106	1.1756	0.4322	2.7202
	4	0.3599	0.1703	−0.4135	0.2091	0.7735	0.2696	2.8691
	2	0.2003	0.0900	−0.2325	0.1110	0.4328	0.1429	3.0277
	1	0.1130	0.0537	−0.1215	0.0612	0.2345	0.0814	2.8806

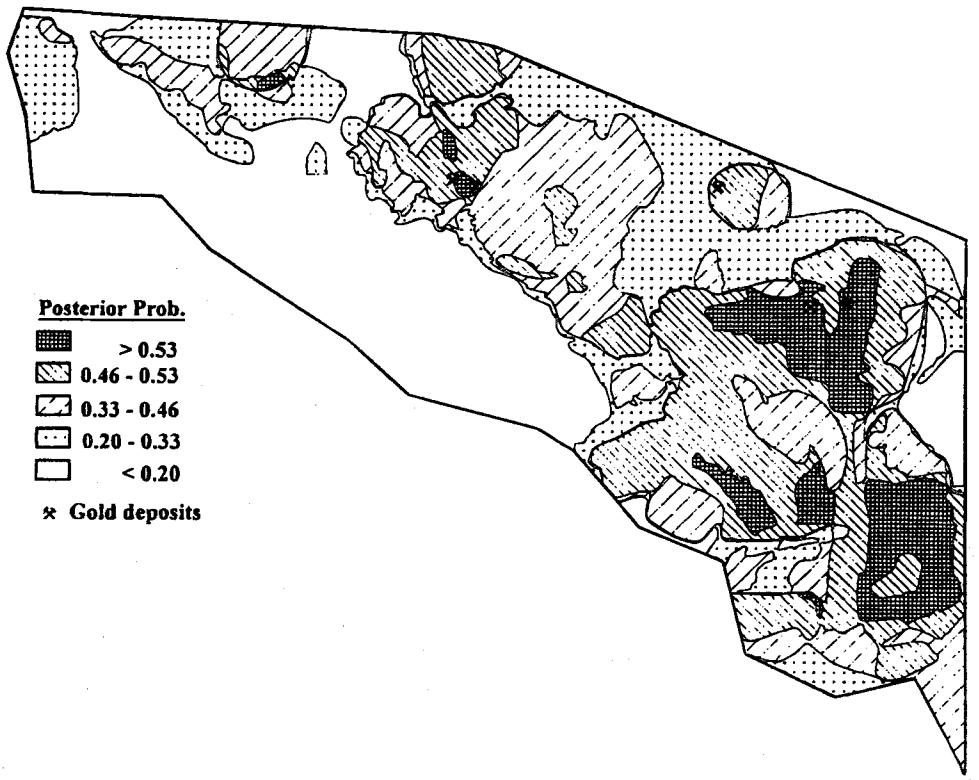

Figure 6. Posterior probability map showing mineral potential for Au in the Iskut River map sheet. The results were obtained by using the parameters in figure 5 and tables 3 and 4 for the binary patterns in figure 4 obtained using cell sizes 4 km.

cell size should be the smallest possible value yielding (a) power-law relations for all patterns, and (b) maximum t-values for the weights. For the present example, 4 km was chosen as the optimum cell size for computing the posterior probability (figure 6). Estimated total numbers of Au mineral occurrences for different cell sizes are given in the log–log plot of figure 7 which shows a power-law relation with exponent $D = 1.3643 \pm 0.023$ and constant $c = 683.899 \pm 30.4$. These results are only slightly different from those previously obtained in figure 3.

CONCLUSIONS

The method introduced in this paper can be applied for nonfractal/fractal pattern integration in mineral potential estimation, and is relatively straightforward to implement by performing box-counting with the aid of GIS. For mineral potential mapping based on fractal patterns, such as the pattern of Au mineral occurrences in the study area, the results of

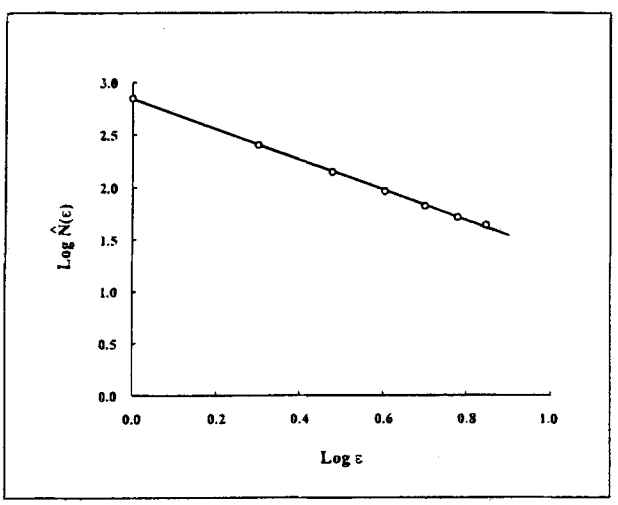

Figure 7. Log–log plot showing the relationships between the estimated total number of mineral occurrences in the study area using the approach introduced in this paper and all cell sizes used for computation.

the estimated posterior probability and the number of mineral occurrences in the study area are significantly related to the value selected for the cell size.

The optimum cell size recommended is the smallest possible value (4 km for the present example) yielding both (a) power–law relations characteristic of fractal patterns, and (b) maximum t-value for the contrast C.

Four indicator patterns (Paleozoic to Mesozoic sedimentary and volcanic clastic rocks, contacts between sedimentary/volcanic clastic and Mesozoic intrusive rocks, linear aeromagnetic anomalies, and geochemical anomalies for Au in stream sediments) were found to be spatially associated with the spatial distribution of Au mineral occurrences and these patterns were integrated for Au mineral potential estimation.

ACKNOWLEDGMENTS

The authors would like to thank the referee Dr. Guocheng Pan, Independence Mining Company, Englewood, Colorado, for helpful comments.

REFERENCES

Agterberg, F. P., 1989, Computer programs for mineral exploration: Science, v. 245, p. 76–81.

Agterberg, F. P., 1992, Combining indicator patterns in weights of evidence modelling for resource evaluation: Nonrenewable Resources, v. 1, no. 1, p. 35–50.

Agterberg, F. P., 1994, Fortran program for the analysis of point patterns with correction of edge effects: Computers & Geosciences, v. 2, p. 229–245.

Agterberg, F. P., and Bonham-Carter, G. F., 1990, Deriving weights of evidence from geoscience contour maps for the prediction of discrete events, *in* Proceedings, 22nd APCOM Symposium held in Berlin, September 1990: Technical University Berlin, v. 2, p. 381–396.

Agterberg, F. P., Bonham-Carter, G. F., and Wright, D. F., 1990, Statistical pattern integration for mineral exploration, in Gaál, G., and Merriam, D. F., eds., Computer applications in resource exploration, prediction and assessment for metals and petroleum: Oxford, Pergamon Press, p. 1–21.

Agterberg, F. P., Cheng, Q., and Wright, D. F., 1993a, Fractal modelling of mineral deposits, *in* Elbrond J., and Tang, X., eds., Application of computers and operations research in the mineral industry, Proceedings, 24th APCOM Symposium, Montreal: Canadian Inst. Mining, Metallurgy and Petroleum Eng., v. 1, p. 43–53.

Agterberg, F. P., Bonham-Carter, G. F., Cheng, Q., and Wright, D. F., 1993b, Weights of evidence modelling and weighted logistic regression for mineral potential mapping: *in* Davis, J. C., and Herzfeld, U. C., eds., Computers in geology–25 years of progress, New Oxford University Press, p. 13–32.

An, P., Moon, W. M., and Rencz, A., 1991, Application of fuzzy set theory for integration of geological, geophysical, and remote sensing data: *Canadian Journal of Exploration Geophysics*, v. 27, p. 1–11.

An, P., Moon, W. M., and Bonham-Carter, G. F., 1992, On a knowledge-based approach of integrating remote-sensing, geophysical, and geological information: *Proceedings IGARSS'92*, p. 34–38.

An, P., Moon, W. M., and Bonham-Carter, G. F., 1994a, Uncertainty management in integration of exploration data using belief function: *Nonrenewable Resources*, v. 3, no. 1, p. 60–71.

An, P., Moon, W. M., and Bonham-Carter, G. F., 1994b, An object-oriented knowledge representation structure for mineral potential estimation: *Nonrenewable Resources*, v. 3, no. 2, p. 132–145.

B. C. Minfile Map 104B, 1989, British Columbia Ministry of Energy, Mines and Petroleum Resources.

Bishop, M. M., Fienberg, S. E., and Holland, P. W., 1975, Discrete multivariate analysis: theory and analysis: Cambridge, MA, MIT Press, 587 p.

Bonham-Carter, G. F., 1994, Geographic information system for geoscientists: modelling with GIS: Oxford, Pergamon, 398 p.

Bonham-Carter, G. F., and Chung, C. F., 1983, Integration of mineral resource data for Kasmere Lake area, northwestern Manitoba, with emphasis on uranium: *Computers & Geosciences*, v. 15, p. 25–45.

Bonham-Carter, G. F., and Wright, D. F., 1989, Weights of evidence modelling: a new approach to mapping mineral potential, *in* Agterberg, F. P., and Bonham-Carter, G. F., eds., Statistical applications in the Earth sciences: Geological Survey of Canada Paper 89-9, p. 171–183.

Bonham-Carter, G. F., Agterberg, F. P., and Wright, D. F., 1988, Integration of geological datasets for gold exploration in Nova Scotia: *Photogrammetry and Remote Sensing*, v. 54, no. 11, p. 1585–1592.

Carlson, C. A., 1991, Spatial distribution of ore deposits: *Geology*, v. 19, February, p. 111–114.

Cheng, Q., 1985, Comprehensive information quantitative appraisal of gold mineral resources in north China Platform: *unpublished MSc thesis*, Changchun University of Earth Sciences (in Chinese with English abstract), 200 p.

Cheng, Q., 1986, A fuzzy integral model for quantitative mineral resource appraisal, *in* Wang, S., ed. & *Journal of Changchun University of Earth Sciences*, special issue (in Chinese with English abstract), p. 35–41.

Cheng, Q., 1989, Multiple population mineral resources simulating method, *in* Wang, S., Fan, J., and Cheng, Q., eds. *Journal of Changchun University of Earth Sciences*, special issue (in Chinese with English abstract), p. 50–59.

Cheng, Q., 1995, Discussion of the perimeter-area fractal model and its application in geology: *Mathematical Geology*, v. 27, no. 1, p. 69–82.

Cheng, Q., 1996, Discrete multifractals: Mathematical Geology, in preparation.

Cheng, Q., and Agterberg, F. P., 1995, Multifractal modelling and spatial point processes: Mathematical Geology, v. 27, no. 7, p. 1–16.

Cheng, Q., and Agterberg, F. P., 1996, Multifractal modelling and spatial statistics: Mathematical Geology, v. 28, no. 1, p. 1–16.

Cheng, Q., and Wang, S., 1990, Comprehensive information mineral resource appraisal: theory and method: *Proceedings 22nd APCOM*, Technical University of Berlin, v. 2, September, p. 397–410.

Cheng, Q., and Agterberg, F. P., 1996, Comparison of two multifractal models: Mathematical Geology, submitted.

Cheng, Q., Agterberg, F. P., and Ballantyne, S. B., 1994a, The separation of geochemical anomalies from background by fractal methods: *Geochemical Exploration*, v. 51, no. 2, p. 109–130.

Cheng, Q., Agterberg, F. P., and Bonham-Carter, G. F., 1994b, Fractal pattern integration for mineral potential mapping: *Proceedings IAMG'94*, Mont-Tremblant, Quebec, October, p. 74–80.

Cheng, Q., Agterberg, F. P., Bonham-Carter, G. F., and Sun, J., 1994c, An artificial intelligence model for integrating spatial patterns for mineral potential estimation with incomplete information: *Proceedings of the 6th Canadian Conference on Geographic Information Systems*, Ottawa, Ontario, v. 1, June 4–10, p. 261–274.

Cheng, Q., Bonham-Carter, G. F., Agterberg, F. P., and Wright, D. F., 1994d, Fractal modelling in the geosciences and implementation with GIS, *Proceedings of the 6th Canadian Conference on Geographic Information Systems*, Ottawa, Ontario, v. 1, June 4–10, p. 565–577.

Cheng, Q., Agterberg, F. P., and Bonham-Carter, G. F., 1995d, A spatial analysis method for geochemical anomaly recognition, *in* Mitri, H. S., ed., Proceedings of CAMT'95 Computer Applications in the Mineral Industry, Montreal, Canada, October 22–25, p. 27–36.

Chung, C. F., and Fabbri, A. G., 1993, The representation of geoscience information for data integration: *Nonrenewable Resources*, v. 2, no. 2, p. 122–139.

Chung, C. F., and Moon, W. M., 1991, Combination rules of spatial geoscience data for mineral exploration: *Geoinformatics*, v. 2, no. 2, p. 159–169.

Coleman, P. H., and Pietronero, L., 1992, The fractal structure of the universe: *Physical Reports (Review Section of Physical Letters)*, v. 213, no. 6, p. 311–389.

Cressie, N. A. C., 1991, Statistics for spatial data: New York, Wiley, 900 p.

Diggle, P. J., 1983, Statistical analysis of spatial point patterns: London, Academic Press, 148 p.

Evertsz, C. J. G., and Mandelbrot, B. B., 1992, Multifractal measures, Appendix B, *in* Peitgen, H.-O., Jürgens, H., and Saupe, D., eds., *Chaos and fractals*: New York, Springer Verlag, p. 922–953.

Feder, J., 1988, *Fractals*: New York, Plenum, 283 p.

Geological Survey of Canada, 1978, Aeromagnetic and gravity data of 104B map sheet: Geophysical Data Centre, Geophysical Division, Geological Survey of Canada.

Geological Survey of Canada, 1988, National geochemical reconnaissance 1:250,000 map sheet, Iskut River, British Columbia (NTS 104B): GSC Open File 1645.

Harris, D. P., 1984, *Mineral resources appraisal*: Oxford, Clarendon Press, 445 p.

Harris, D. P., and Pan, G., 1991, Consistent geological areas for epithermal gold–silver deposits in the Walker Lake Quadrangle of Nevada and California: delineated by quantitative methods: Economic Geology, v. 86, p. 142–165.

Mandelbrot, B. B., 1983, *The fractal geometry of nature*. San Francisco, W. H. Freeman and Company; New York, updated and augmented edition, 468 p.

McCammon, R. B., Botbol, J. M., Sinding-Larsen, R., and Bowen, R. W., 1983, Characteristic analysis—1981: final program and a possible discovery: Mathematical Geology, v. 15, no. 1, p. 59–83.

Ripley, B. D., 1981, Spatial statistics: New York, Wiley, 252 p.

Ripley, B. D., 1988, Statistical inference for spatial processes: Cambridge, Cambridge University Press, 148 p.

Wang, S., Cheng, Q., and Fan, J., 1990, Methods for gold mineral resources appraisal: Jilin, P. R. China, Press of Jilin Sci. & Tech. (in Chinese), 441 p.

Wright, D. F., and Bonham-Carter, G. F., 1996, VMS facorability mapping with GIS-based interpretation models, Chisel-Anderson map area, Manitoba, *in* Bonham-Carter, G. F., Galley, A. G., and Hall, G. E. M., eds., EXTECH I: A multidisciplinary approach to massive sulphide deposits in the Rusly Lake—Snow Lake greenstone belts: Geological Survey of Canada, Bulletin, in press.